Int J Earth Sci (Geol Rundsch) (2016) 105:1591–1602
DOI 10.1007/s00531-015-1272-1

ORIGINAL PAPER

Structural interpretation of the Chuan-Dian block and surrounding regions using discrete wavelet transform

Songbai Xuan[1] · Chongyang Shen[1] · Hui Li[1] · Hongbo Tan[1]

Received: 4 February 2015 / Accepted: 24 October 2015 / Published online: 13 November 2015

Abstract The Chuan-Dian tectonic block is a transitional zone between the Tibetan Plateau and the South China block. The crustal structure in this region has been studied in several ways, and in this work we present Bouguer gravity anomaly data with which to investigate the Chuan-Dian block and surrounding regions. Regional and local anomalies are decomposed using a method of discrete wavelet transform (DWT), and furthermore, the relief of the Moho is inverted based on the regional anomalies. Results of the transform show that there is a distinct belt of regional anomalies on the east and southeast margins of the Tibetan Plateau. In addition, there are two distinct gradient belts evident in the maps of the local gravity anomalies. The first of these, in the western Indo-China block, has a north–south strike with high anomalies around this belt, and the second is along the Longmenshan fault zone in the eastern margin of the Tibetan Plateau. The Chuan-Dian block can be divided into two discrete parts, separated by a broad and indistinct boundary observed from the fifth-order DWT detail and Moho relief. The DWT details reveal that parallel anomalies existing in the Indo-China block region were induced by subduction of the Burmese block. We conclude that the clockwise rotation of the Chuan-Dian block was synthetically affected by the extrusion of the Tibetan lithosphere and subduction of the Burmese block.

✉ Songbai Xuan
song_bai_whu@163.com

[1] Key Laboratory of Earthquake Geodesy, Institute of Seismology, China Earthquake Administration, Wuhan 430071, China

Keywords Bouguer gravity anomalies · Discrete wavelet transform · Crustal structure · Moho relief · Chuan-Dian block

Introduction

The use of gravity methods in geophysics plays an important role in being able to interpret current crustal structure. It is widely known that gravity anomalies are composed of various components, responsible for different scales and source depths. Several techniques have been developed to decompose the gravity anomalies and characterize their sources. Discrete wavelet transform (DWT), based on Mallat's theory (1989), is one of the most powerful tools, and has been applied to their interpretation of gravity data in terms of crustal structure. Yang et al. (2001) introduced the theory for separation of the gravity anomalies using DWT in detail, and analyzed gravity data obtained from across China. Wu et al. (2011) inverted the crustal thickness in the northeastern Tibetan Plateau based on the fourth-order DWT approximation of Bouguer gravity anomalies (BGA). Lou and Wang (2005), Xu et al. (2009), Jiang et al. (2011) and Evariste et al. (2014) combined DWT and spectrum analysis to interpret the crustal structure beneath Sichuan–Yunnan, Dagang, Beijing and Cameroon, respectively. Xuan et al. (2012) applied DWT to analyze the mechanism of change in gravity from 2000 to 2007 in mainland China. Most recently, Oruç (2014) proposed an effective technique to reflect sources edges obtained using DWT, based on the square root of the sum of the squares of the horizontal, vertical and diagonal components.

The Chuan-Dian block (CDB), located in southwestern China, is bounded by the Xianshuihe–Xiaojiang fault system, Jinshajiang suture zone and Red River fault, as shown

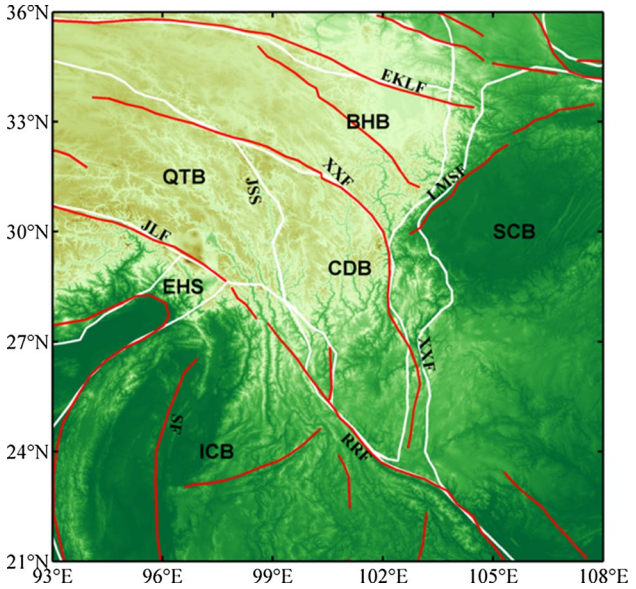

Fig. 1 Regional topography, crustal blocks (bounded by *white lines*) and principal active faults (shown in *red*) of the study area (after Tapponnier et al. 1977, 2001; Deng et al. 2002). Abbreviations as follows: *ICB* Indo-China block, *QTB* Qiangtang block, *CDB* Chuan-Dian block, *BHB* Bayan Har block, *SCB* Sichuan Basin, *EHS* Eastern Himalayan Syntaxis, *JSS* Jinshajiang suture, *EKLF* East Kunlun fault, *XXF* Xianshuihe–Xiaojiang fault system, *LMS* Longmenshan fault, *RRF* Red River fault, *SF* Sagaing fault

in Fig. 1 (Deng et al. 2002; Zhang et al. 2005). It is tectonically active and forms the transitional zone between the uplifted Tibetan Plateau to the west and the Yangtze continental platform to the east. The collision between the Indian and Eurasian plates ~50 Ma ago resulted in strong deformation, regmagenesis and formation of complex Cenozoic structures (Yin and Harrison 2000). However, debate about the deformation of this region has centered on whether extrusion tectonics has been largely accomplished by rigid block motion (Leloup et al. 1995) or associated with distributed deformation (Burchfiel et al. 1995). The southeast borderland (plateau margin) of the Tibetan Plateau lacks a distinct edge and little evidence of shortening in the upper crust (Clark et al. 2000, 2005; Shoenbohm et al. 2006). Using the Global Positioning System (GPS) to track movement suggests that the CDB rotates clockwise around the Eastern Himalayan Syntaxis (Zhang et al. 2004; Shen et al. 2005; Wang et al. 2008). Thus, lateral extrusion of the crustal block (Tapponnier et al. 1977, 1982, 2001) and lower crustal flow (Royden et al. 1997; Clark et al. 2000, 2005; Shoenbohm et al. 2006) have been proposed to explain the tectonic deformation and movement in this region.

In this work, we present the results of reprocessed BGA data of the CDB, and adjacent region, derived from EGM2008 (Pavlis et al. 2012) using the DWT method to investigate the validity of these claims as they pertain to the crustal structure, and therefore tectonic history of the CDB.

Methodology

Discrete wavelet transform

Based on the theory of Mallat (1989), the processing of the DWT includes wavelet decomposition and reconstruction of the data. The wavelet basis, or the mother wavelet function $\psi_{a,b}(x)$, is defined by scale and shift as follows:

$$\psi_{a,b}(x) = \frac{1}{\sqrt{a}}\psi\left(\frac{x-b}{a}\right) \tag{1}$$

where a and b are the continuously varying scaling and shifting parameters, respectively. Assuming that $g(x)$ is the gravity signal, its wavelet transform may be expressed using Eq. (1) as:

$$w(a,b) = \frac{1}{\sqrt{a}}\int_{-\infty}^{\infty} g(x)\psi\left(\frac{x-b}{a}\right)\mathrm{d}x \tag{2}$$

where Eq. (2) is essentially the wavelet decomposition of $g(x)$ by means of the wavelet basis or the mother wavelet function $\psi_{a,b}(x)$. If the parameters a and b in Eq. (1) take discrete values, Eq. (2) is the function of the DWT.

Corresponding to an orthogonal base, the original data can be decomposed as an approximation (A), and with details according to three orientations: horizontal ($D^{(h)}$), vertical ($D^{(v)}$) and diagonal ($D^{(d)}$) components using a two-dimensional (2D) DWT. Figure 2 shows the basic steps of wavelet decomposition and construction of the jth order in which the jth-order approximation A_j may be decomposed to the j^{+1}-order approximation coefficient CA_{j+1}, with detail coefficients $CD^{(h)}_{j+1}$, $CD^{(v)}_{j+1}$ and $CD^{(d)}_{j+1}$. The approximate and detail coefficients form a representation with half the resolution of the data at level j. Using the algorithm given by Mallat (1989) for reconstructing the original signal from its decomposition, the wavelet approximation A_{j+1} details at level $j+1$ can be reconstructed according to three orientations: horizontal $D^{(h)}_{j+1}$, vertical $D^{(v)}_{j+1}$ and diagonal $D^{(d)}_{j+1}$. Therefore, the wavelet detail D_{j+1} at level $j+1$ is the sum of the horizontal, vertical and diagonal components. The wavelet approximation A_j at level j is the sum of A_{j+1} and D_{j+1}. The wavelet approximation and wavelet detail at the $j+1$ level have the same resolution as $A_j$at the j level. The iterative process described above is continued until the desired results are achieved.

Yang et al. (2001) suggested that the decomposition can be operated. Based on the low-order wavelet detail invariant rule, the gravity data can be separated into regional and residual anomalies by using the 2D DWT arbitrarily

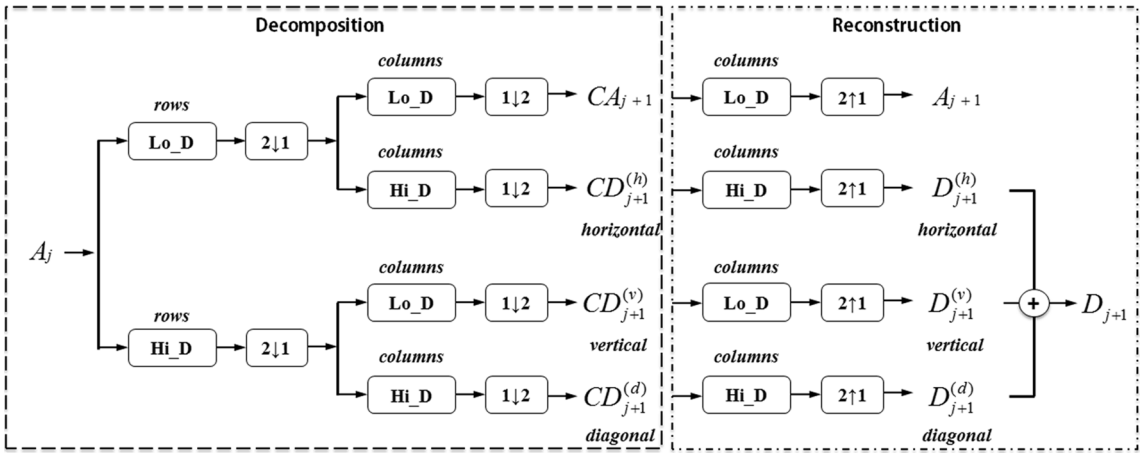

Fig. 2 Diagrammatic representation of the basic calculation steps used in the discrete wavelet transform (DWT) at level *j*, where A_j is wavelet approximation at level *j*. The steps of the decomposition and reconstruction are shown in the *dotted box* on the *left* and *right*, respectively. The wavelet coefficients *CA* (approximation coefficient) and *CD* (detail coefficient) are also shown

according to the requirements. If the *n*th-order approximation meets our requirements, we can take it as the regional anomalies, while the local anomalies are the sum of the details from the first- to the *n*th-order equivalent to the regional anomalies removed from the original data.

Synthetic testing

A combination model was designed (Fig. 3a) for synthetic testing to prove the feasibility of the DWT method. The main parameters of the synthetic model are listed in Table 1. This model consists of five prisms: Four small prisms are located relatively shallow (6.5 km), and one larger prism is located at a greater depth (50 km). Using forward calculation in the frequency domain, as proposed by Parker (1972), we calculated the gravity anomalies of the model and the corresponding anomalies induced by shallow and deeper prisms, respectively. Gravity anomalies induced by the shallow prisms (1–4) are shown in Fig. 3b and that of the deeper prisms (5) in Fig. 3c. Figure 3d shows the total gravity anomaly induced by the test model.

The first- to fifth-order DWT details are shown in Fig. 4, with approximations after decomposition and reconstruction. The first-order detail (Fig. 4a) may be considered noise from forward calculation, and thus, the first-order approximation (Fig. 4a′) can be described as the gravity anomaly determined by noise reduction from the total anomaly (Fig. 3d). The anomalies induced by the shallow prisms are obvious, and almost no signal is induced by the deeper prism in the second- to fourth-order DWT details. However, the gravity anomalies induced by the deeper prism are evident in the fifth-order DWT details. This indicates that the subsurface anomaly bodies are not continuous, unlike the synthetic model, and the local and regional anomalies separated using the DWT method shown in Fig. 5 are very similar to the calculated anomalies (Fig. 3b, c) such that the local anomalies (Fig. 5a) are the sum of the first- to the fifth-order DWT details, i.e., the main anomalies are induced by the shallow prisms. However, the anomalies induced by the deeper prism are also displaced and appear different to the calculated anomalies as shown in Fig. 3b. The gravity anomalies in Fig. 5b are almost entirely induced by the deeper prism. Thus, the sum of the first- to the fifth-order DWT details (Fig. 5a) and the fifth-order DWT approximation (Fig. 5b) could be considered the local and regional fields, respectively. Overall, it is evident that the DWT method yields satisfactory separation results compared with the theoretical anomalies and can be considered feasible to separate anomalies of different scales.

Gravity analysis

The BGA used here, derived from the EGM2008 spherical harmonic coefficients (Pavlis et al. 2012), were downloaded from the webpage of the Bureau Gravimétrique International (http://bgi.omp.obs-mip.fr). In this database, a terrain correction is applied up to a distance of 167 km using the 1 arcmin by 1 arcmin ETOPO1 digital elevation model, and a density reduction of 2.67 g/cm^3 is also applied.

In general, Bouguer gravity data can reflect the large-scale tectonic feature directly. As shown in Fig. 6, the general BGA in the east and southeast margins of the CDB are characterized by NW–SE and N–S trends, respectively. The map reveals a broad regional negative BGA in the Tibetan Plateau, including the Bayan Har block, Qiangtang block and northern CDB. Such a negative BGA could have resulted from material depletion during the crustal thickening around the eastern Tibetan Plateau. Larger anomalies

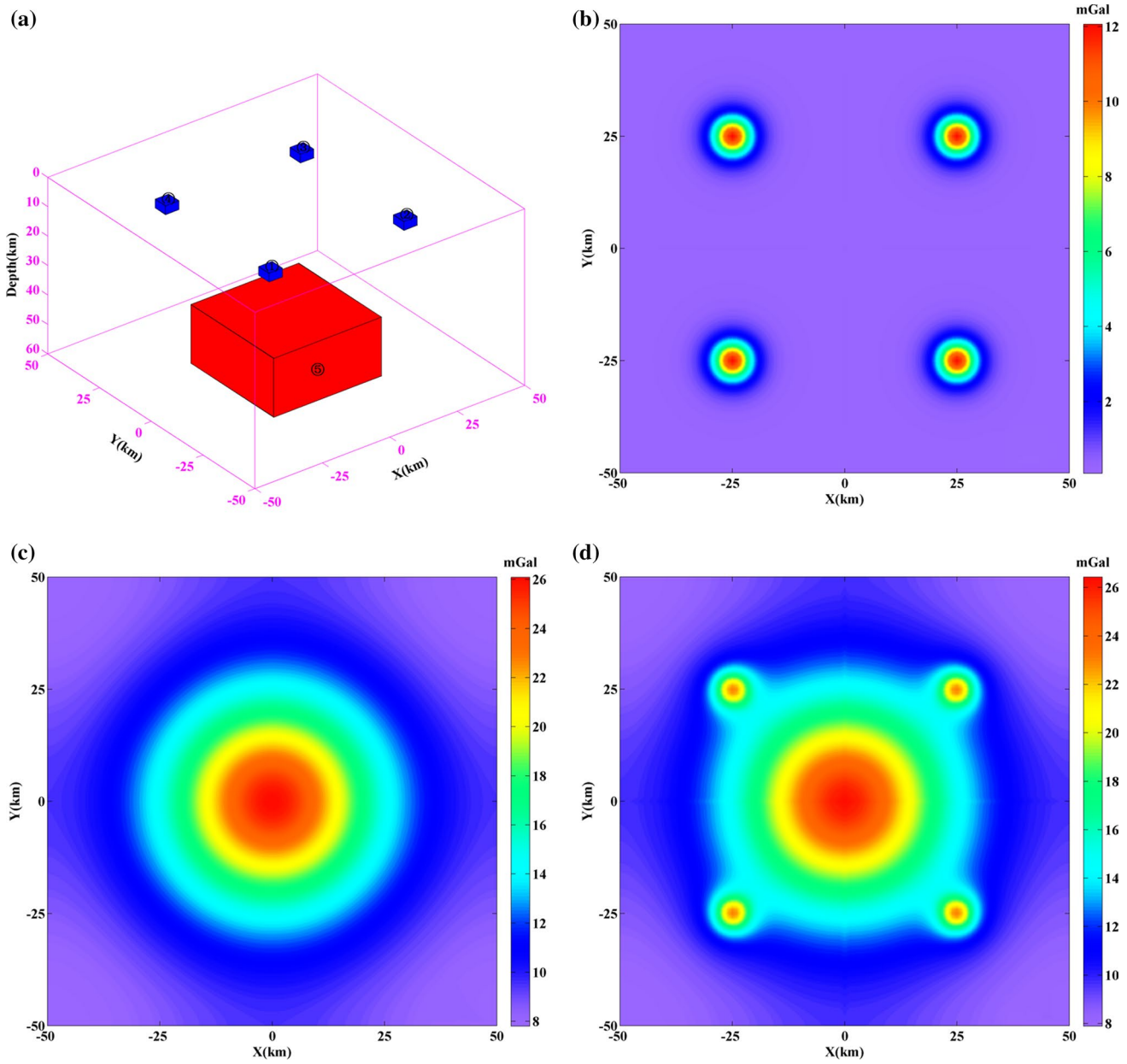

Fig. 3 **a** Synthetic gravity model with the prisms 1–4 used to represent shallow density anomaly bodies and prism 5 as a single, deeper density anomaly body. **b** Gravity anomalies induced by prisms 1–4 and **c** gravity anomalies induced by the prism 5. **d** Total gravity anomalies induced by the test model

Table 1 Main synthetic model input parameters

Model	Center coordinate (km)			Size (km)			Density contrast (g/cm^3)
	x	y	z	x	y	z	
①	−25	−25	6.5	5	5	3	0.4
②	25	−25	6.5	5	5	3	0.4
③	25	25	6.5	5	5	3	0.4
④	−25	25	6.5	5	5	3	0.4
⑤	0	0	50	40	40	20	0.4

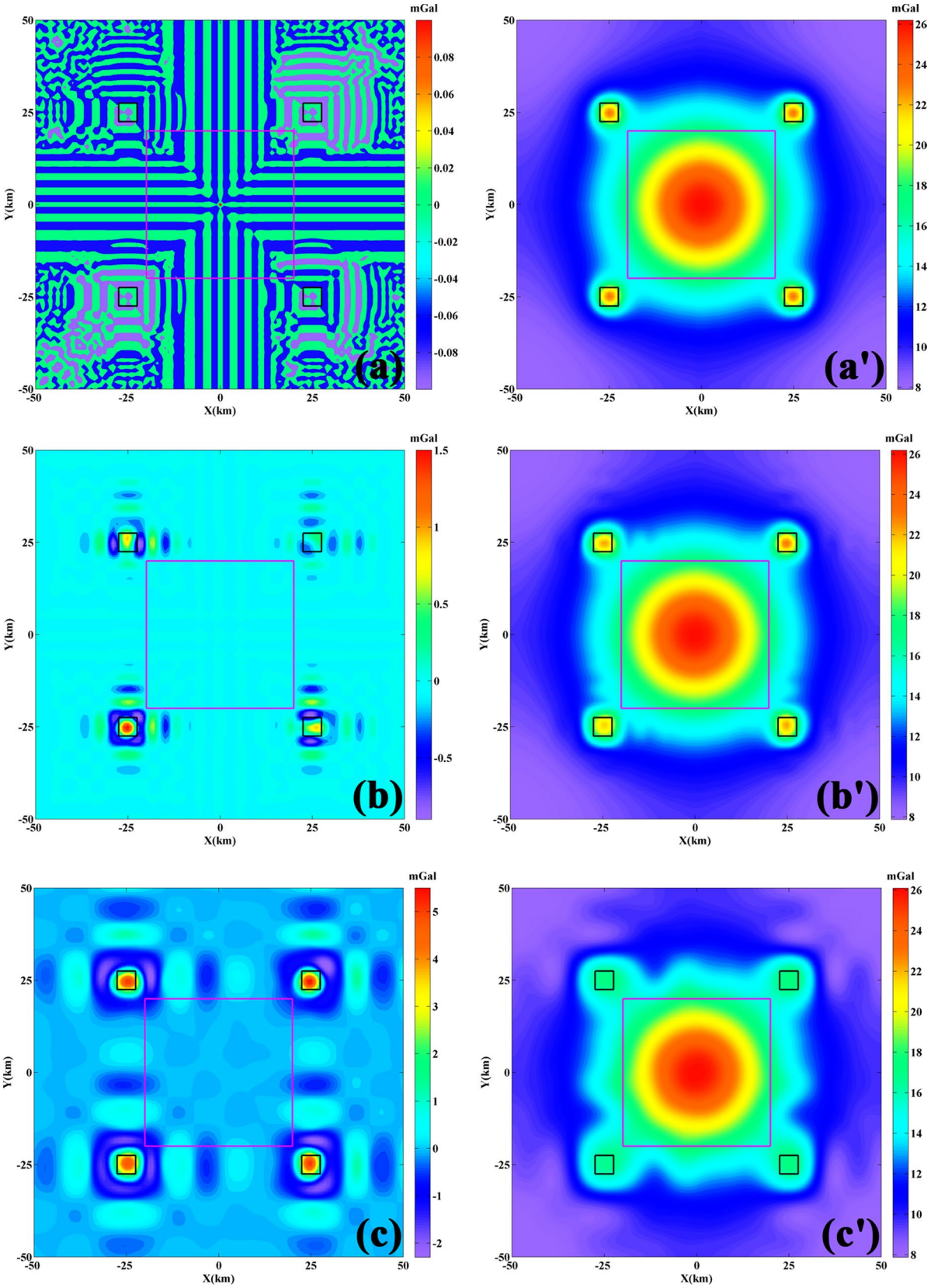

Fig. 4 Results of the 2D DWT decomposition. **a**–**e** Details of the first-order to fifth-order 2D DWT decomposition (results of **a** may be considered noise from forward calculation). **a′**–**e′** first- to fifth-order 2D approximation, in which **a′** can be described as the anomaly determined by noise reduction from the total anomaly. The *black outlined squares* and *magenta outlined squares* are the edge projections of the shallow prisms and deeper prism, respectively

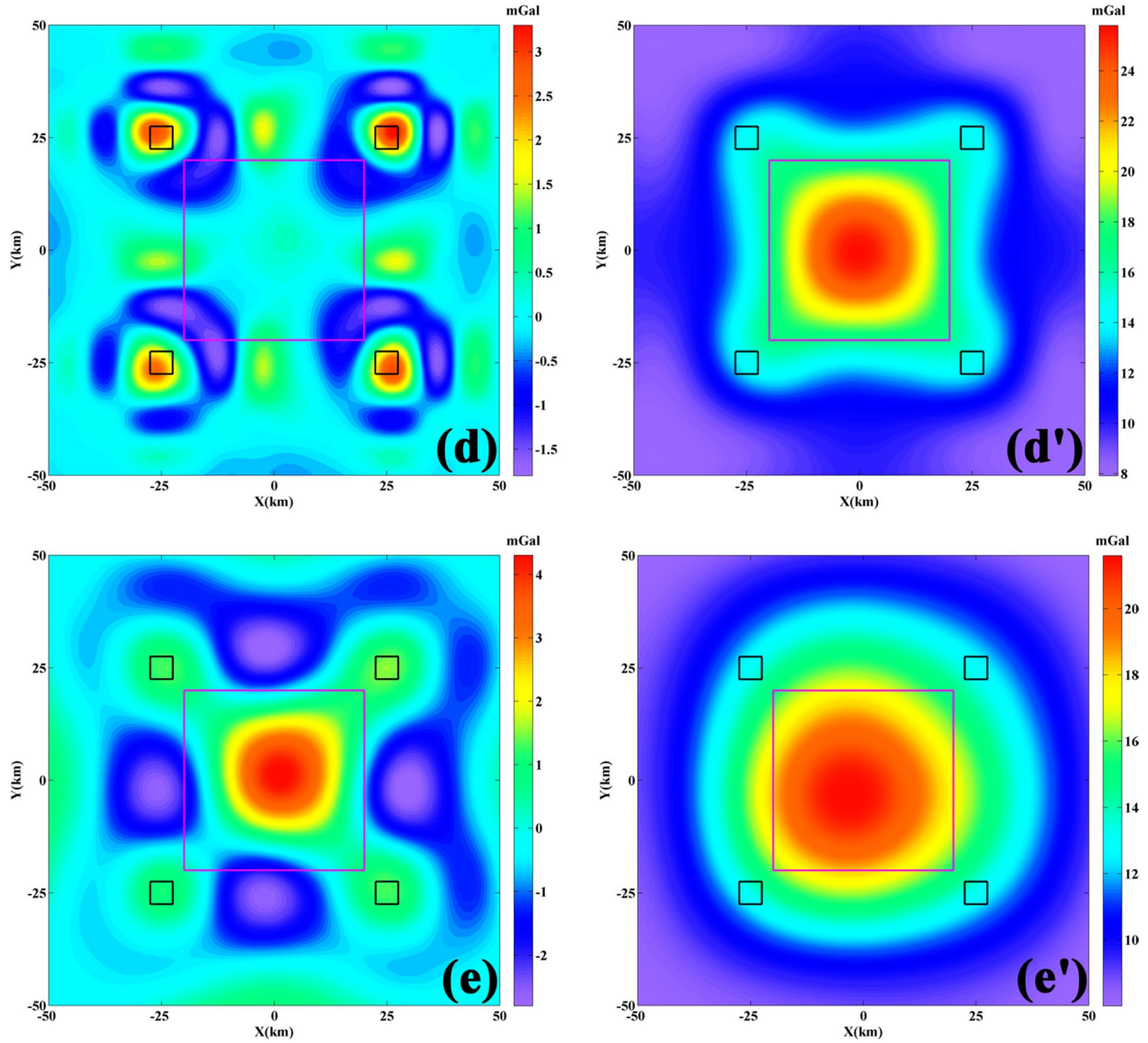

Fig. 4 continued

(~−100 mGal) exist in the Sichuan Basin and near the Sagaing fault south of the Eastern Himalayan Syntaxis. The maximum and minimum BGA are 0.7 and −559.3 mGal, respectively. There are two distinct gravity gradient belts: one in a NE–SW direction along the Longmenshan fault zone and the other in a NW–SE direction along the Jiali fault of the Eastern Himalayan Syntaxis. Although these two fault zones form the main borders of the Tibetan Plateau, the southeast margin is not very clear and is expected to be outlined by BGA of between −300 and −200 mGal.

Results of multi-scale BGA decomposition

Figure 4 shows that 2D DWT decomposition of BGA (Fig. 6) distinguishes regional and local anomalies. Given that we selected the fifth-order 2D DWT approximation as regional anomalies (Fig. 7a), it is evident that the map of regional anomalies reveals the margins of the Tibetan Plateau more smoothly than BGA, and so the boundaries of the blocks, such as the Indo-China block and Sichuan Basin, can be identified more easily. The belt with anomalies between −400 and −300 mGal calibrates well with the east and southeast margins of the Tibetan Plateau. Therefore, the CDB may be divided into two portions on a regional scale: the southwestern Sichuan and the middle Yunnan.

From Fig. 7b, it is observed that the low anomalies strike in an N–S direction around the western Indo-China block and are bounded by relatively high anomalies suggesting that the crustal deformation here, from continental

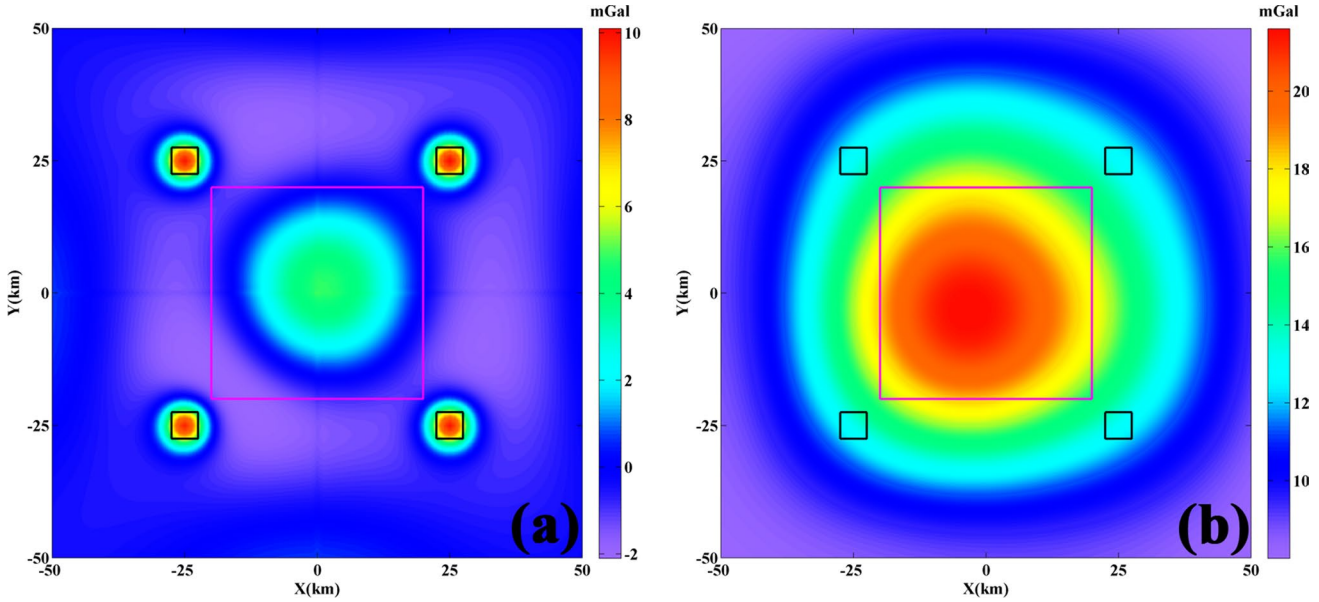

Fig. 5 **a** Local and **b** regional anomalies determined using the 2D DWT method. The local anomalies are the sum of the first-order to fifth-order DWT details and the regional anomalies are the fifth-order DWT approximation

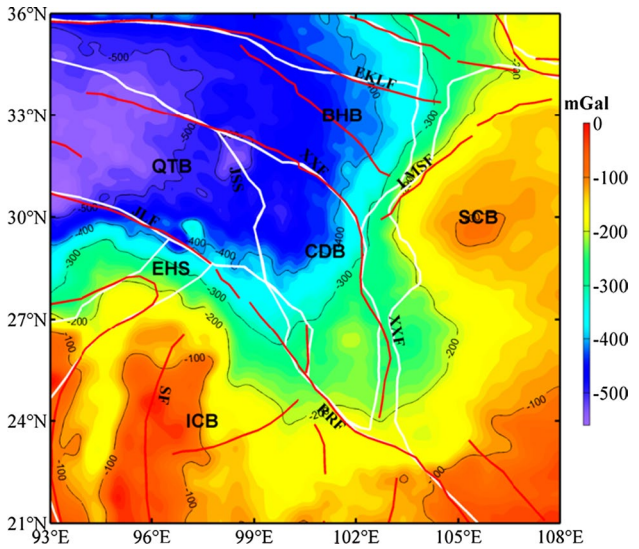

Fig. 6 Bouguer gravity anomalies (BGA) superimposed the main crustal blocks (bounded by *white lines*) and active faults (*red lines*) of the Chuan-Dian block and surrounding regions (see Fig. 1 for key to abbreviations)

collision, is intense. Another apparent gradient belt is the Longmenshan fault belt of the eastern margin of the Tibetan Plateau. The NE trending high anomaly lies along the Longmenshan fault, and a low anomaly is located in the eastern part of the Bayan Har block. The different gravity anomalies may have resulted from differential movement of the crust in the eastern Tibetan Plateau and around the northern and southern parts of the CDB; the low and high anomalies are separated by the Xiaojinhe fault.

The fourth-order detail map (Fig. 8a) reveals the density structure of the upper crust. Gravity anomalies are complex, reflecting the complex density structures in the middle crust. It is evident that a high-gravity anomaly exists beneath the Jinshajiang suture near the western boundary of the CDB and a low-gravity anomaly exists beneath the Jiali fault. The parallel anomalies in the southwestern region of the study area imply strong deformation in the lower crust, induced by eastward extrusion of the Burmese block and clockwise rotation of the CDB around the Eastern Himalayan Syntaxis.

The fifth-order detail map (Fig. 8b) reveals the density structure of the lower crust. The local anomalies and the fifth-order details mainly result from inhomogeneity in the density distribution of the whole and lower crust, respectively. In the Indo-China block and Eastern Himalayan Syntaxis, eastward arcs of lower and high anomalies indicate that subduction of the Burmese block occurs in the lower crust, a phenomenon that is not obvious in the middle crust (Fig. 8a). Similar to the local anomalies (Fig. 7b), gravity anomaly images clearly highlight the differences between the northern and southern portions of the CDB. In the Longmenshan region, high anomalies strike along the Longmenshan fault, and low anomalies exist in the northeastern area of the Longmenshan fault, suggesting that the effects of the eastward extrusion of the Bayan Har block exist in the lower crust.

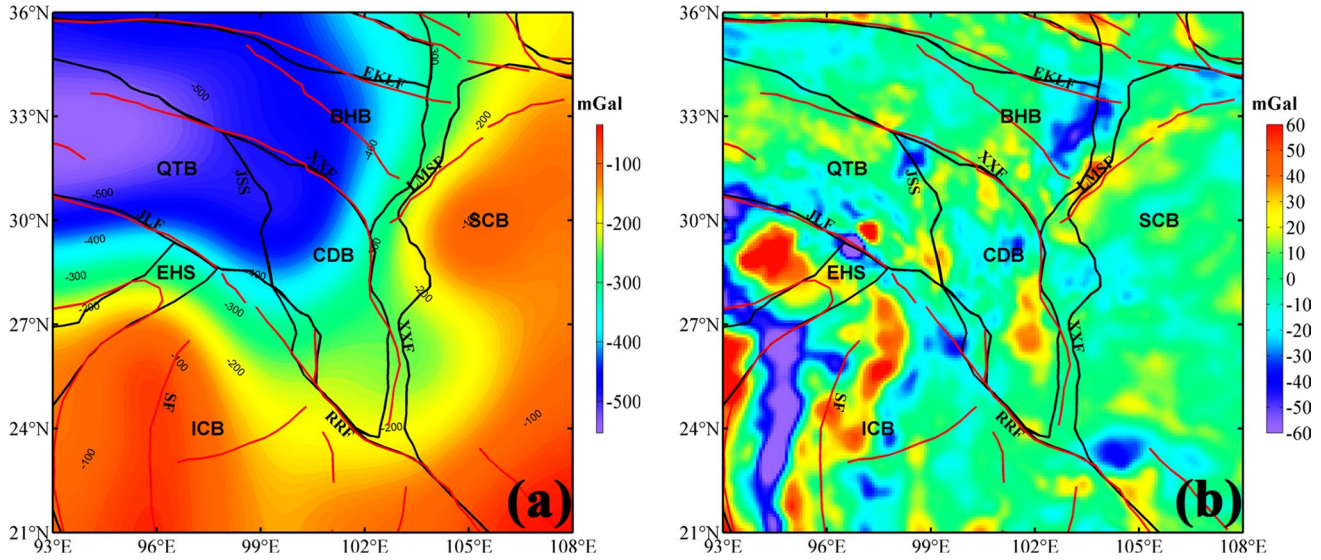

Fig. 7 **a** Regional and **b** local gravity anomalies of Chuan-Dian region separated using the DWT method. The regional anomalies are the fifth-order DWT approximation, and the local anomaly is the product of removing the regional anomalies from the BGA shown in Fig. 3

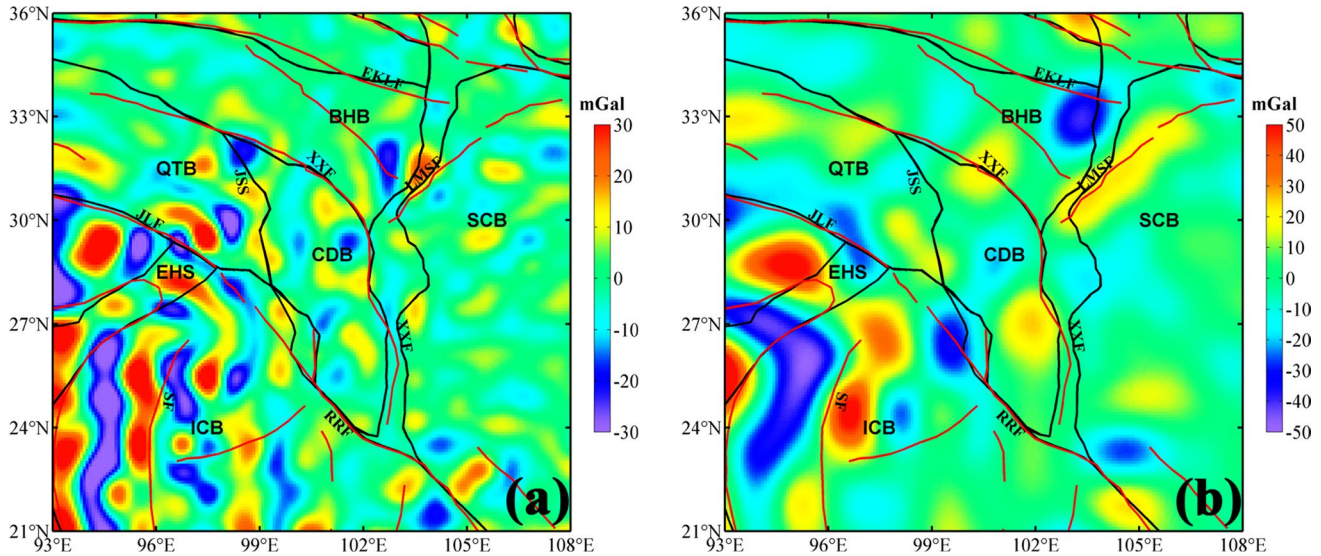

Fig. 8 Maps showing **a** fourth-order and **b** fifth-order DWT details of the BGA for the Chuan-Dian region

Relief of the Mohorovicic discontinuity

The morphology of the Mohorovicic discontinuity (Moho) is fundamental for interpretation of crustal structure and tectonic activity. The inversion method used in this work is based on the Parker–Oldenburg algorithm (Parker 1972; Oldenburg 1974) which requires knowledge of the reference depth and the density contrast between the crust and mantle. A reference depth of 50 km and density contract of -0.4 g/cm^3 are used here, in agreement with the average values reported in the CRUST1.0 model of Laske et al. (2013).

Using the regional anomalies (Fig. 7a), the reference depth and the density contrast, the relief of the Moho with standard deviation of 0.079 mGal after seven iterations was obtained (Fig. 9a). The gravity anomalies produced by the Moho relief shown in (Fig. 9b) are similar to the regional anomalies (Fig. 7a). Notably, the final residuals from adjusting the regional anomalies using gravity anomalies induced by Moho relief have a normal distribution with a mean of -1.891 mGal and standard deviation of 12.564 mGal (Fig. 9c), and the majority of the grid points have a low residual value. Therefore, the result of the Moho relief analysis is considered credible.

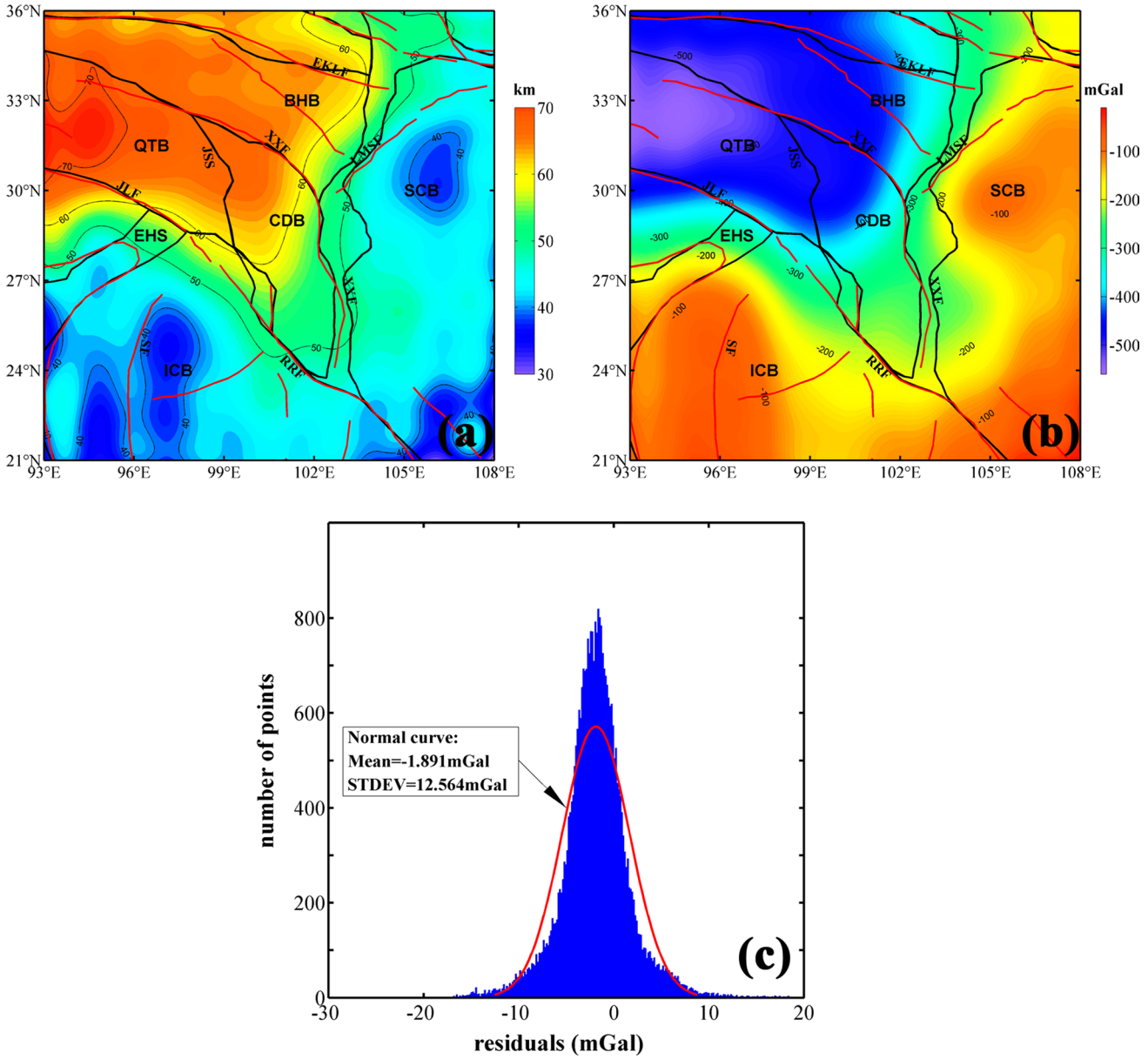

Fig. 9 **a** Map showing the relief of the Moho derived from regional anomalies (Fig. 7a). **b** Map of the calculated anomalies induced by the relief the Moho and **c** statistical analysis of final gravity residuals induced by Moho relief showing a normal distribution

There is a significant change in the depth of the Moho undulation between the Tibetan Plateau and the surrounding regions (Fig. 9a). The obvious steep belt of deep Moho appears in both the Longmenshan fault and the Eastern Himalayan Syntaxis. The depth of the Moho on both sides of the Longmenshan fault drops from nearly 70 km to less than 50 km from northwest to southeast. There are abnormal belts parallel to the Longmenshan fault at a depth of 65 km in the northwest and 30–44 km in the Sichuan Basin to the southeast. The depth of the Moho is approximately 60 km in the northern portion of the CDB and approximately 50 km in the southern portion, reaching a depth of approximately 70 km in the Qiangtang block. On both the west and east side of the Sagaing fault, the depth of the Moho is less than 40 km. In the south segment of the Xianshuihe–Xiaojiang fault system, the depth increases from 50 to 55 km in the west. From the west, near the Eastern Himalayan Syntaxis across the middle of the CDB, to the east (the Longmenshan fault region), the Moho has a Y-shaped relief. In conjunction with the topography belt, this suggests that the CDB is a transitional zone of the Tibetan Plateau, the South China block and the Indo-China block.

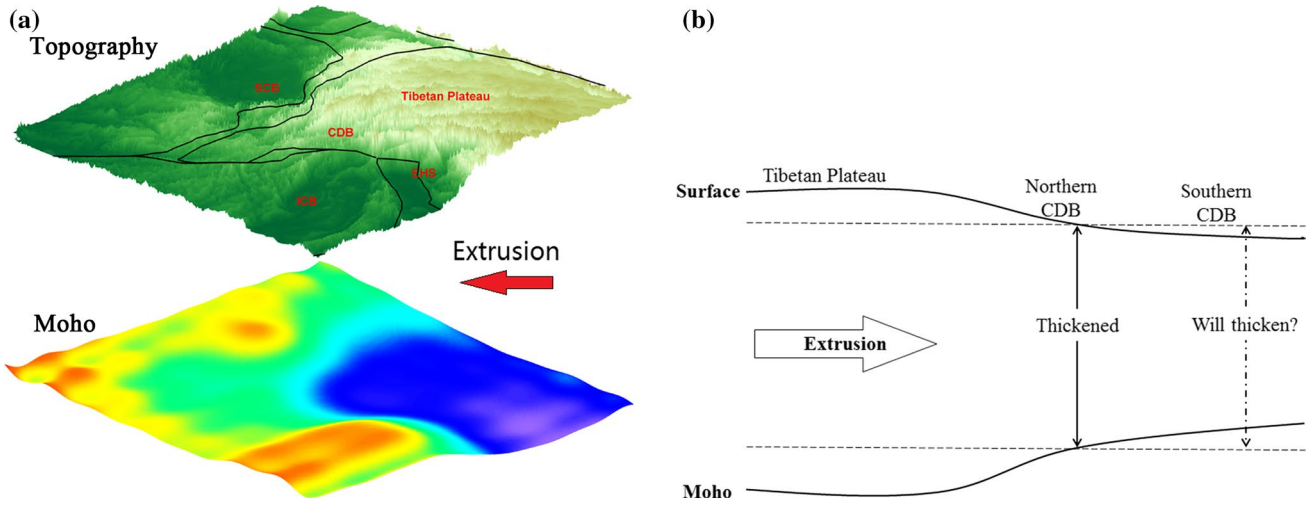

Fig. 10 **a** 3D map view of the regional topography and underlying Moho relief indicating the extrusion direction of the Tibetan Plateau (*red arrow*). **b** Schematic N–S cross section showing the extrusion direction of the Tibetan Plateau and crustal subdivisions of the northern and southern Chuan-Dian block

Discussion

The regional and local gravity anomalies separated from the BGA in the CDB and surrounding regions (Fig. 7) closely correlate with the regional tectonic setting. The study area can be divided into four parts according to gradient belts of the regional anomalies (Fig. 7a). These are the Tibetan Plateau, southern CDB, Sichuan Basin and Indo-China block. The morphology of the gradient belt generally accords with the strike direction of the Longmenshan fault, the south segment of the Xianshuihe–Xiaojiang fault, the Jiali fault and the Red River fault. The local anomalies (Fig. 7b) and fourth- and fifth-order details (Fig. 8) suggest that the complex structural character of the crust of the CDB and surrounding regions was affected by eastward extrusion of the Tibetan lithosphere (Tapponnier et al. 1982, 2001).

The regional negative anomalies were probably induced by crustal thickening (Fig. 9b; Molnar et al. 1993). During southeastward movement of the Tibetan Plateau (Zhang et al. 2004; Shen et al. 2005; Wang et al. 2008), crustal material was injected into the region between the Sichuan Basin and Indo-China block, a broad and indistinct southeastern margin to the Tibetan Plateau (Clark et al. 2000, 2005; Shoenbohm et al. 2006). This margin results in the gravity anomalies of between −400 mGal in the northwest part and −300 mGal in the southeast part of the CDB, indicating that the extruded Indo-China block and South China block (Tapponnier et al. 1982; Ji et al. 2008) are affected by southeastward wedging of the CDB. The crust of the Tibetan Plateau is still in a strongly non-isostatic state (Wang et al. 2009), and thus, the southeastward extrusion leads to surficial uplift and subsidence of the Moho (Clark et al. 2000), resulting the formation of significant differences in Moho topography (Fig. 9a) and crustal thickness (Fig. 10a) in the northern CDB. The continuous southeastward extrusion would also tend to increase the crustal thickness in the southern CDB, much the same as the northern CDB (Fig. 10b). However, without the obstruction of resistive blocks (e.g., Sichuan and Tarim) in the wave of extrusion, it is not clear whether the crust of the southern CDB would thicken to greater than 60 km with time, as is the case for the northern CDB (Fig. 10b). Therefore, the CDB can be divided into two parts in terms of extrusion and crustal thickness: the northwestern and southeastern part. Although the two parts of the CDB rotate clockwise around the Eastern Himalayan Syntaxis (Wang et al. 2008, 2014), their angular velocities are different, as observed from the results of GPS tracking (Shen et al. 2005).

The eastward extruded Tibetan lithosphere is expected to change direction toward the south and southwest because of resistance from the Sichuan Basin within the NE trending margin. Eastward arcs of negative and positive anomalies (Fig. 8b) and 40–50 km Moho relief (Fig. 9a) near the Eastern Himalayan Syntaxis suggest that the effects of subduction of the Burmese block in the lower crust (Socquet and Pubellier 2005; Wang et al. 2007) spread to the CDB. Thus, movement toward the south and southwest would cause the CDB to rotate clockwise around the Eastern Himalayan Syntaxis along the strike-slip faults (Royden et al. 1997; Wang et al. 2008). Multiple-order *en echelon* patterns of positive and negative anomalies across the Indo-China block from west to east (Figs. 7b, 8a, b) suggest that the crust is folded, much like the results of plasticine simulations by Tapponnier et al. (1982), given the anticipated

rheological behavior of the lower crust (Wang et al. 2007; Bai et al. 2010).

Unlike the Indo-China and Eastern Himalayas, the eastern margin of the Tibetan Plateau, i.e., Longmenshan fault, is a thrust-nappe structure. The Bayan Har block, situated between the East Kunlun fault and the Xianshuihe fault, is moving toward the southeast. The eastern Bayan Har block is divided into the Longmenshan sub-block (between 102°E and Longmenshan fault) and the Aba sub-block (west 102°E) by the right-lateral strike-slip Longriba fault, which strikes NW–SE (Xu et al. 2008; Jiang et al. 2012). The anomalies of the fifth-order DWT details (Fig. 8b) in the Longmenshan sub-block are negative, indicating that the southeastward extrusion of the Bayan Har block is resisted intensely by the Sichuan Basin, resulting in the Longmenshan mountain uplift and southwestward flow of lower crustal matter along the Longmenshan fault (Clark et al. 2000). The positive anomalies along the Longmenshan fault in the fifth-order DWT details (Fig. 8b) suggest that such material may be accumulated in the lower crust.

Conclusions

The discrete wavelet transform provides an effective method for interpreting the crustal structure based on gravity data. Regional and local anomaly analysis of the crustal structure and inverted Moho relief of the CDB, and surrounding regions shows that the Chuan-Dian region is closely correlated with the tectonic activities of the eastern Tibetan Plateau and the Eastern Himalayan Syntaxis. There are significant differences in crustal structure between the northern and southern portions of the CDB, from the local anomalies (Fig. 7b), the fifth-order detail (Fig. 8b) and Moho depth (Fig. 9a), supporting the division into two sub-blocks by fault zones and providing a good indication of the regional tectonic setting. The topography, crustal structures and tectonic activities appear to mainly result from the eastward extrusion of the Tibetan lithosphere and eastward subduction of the Burmese block.

Acknowledgments The authors thank the Bureau Gravimétrique International (BGI) for supplying the Bouguer gravity anomaly data. This work was financially supported by the Foundation of Institute of Seismology, China Earthquake Administration (Grant No. IS201326122) and the National Natural Science Foundation of China (Grant No. 41304060) and the National key Basic Research Program of China (Grant No. 2013CB733305).

References

Bai D-H, Unsworth MJ, Meju MA, Ma X-B, Teng J-W, Kong X-R, Sun Y, Sun J, Wang L-F, Jiang C-S, Zhao C-P, Xiao P-F, Liu M (2010) Crustal deformation of the eastern Tibetan plateau revealed by magnetotelluric imaging. Nat Geosci 3(5):358–362

Burchfiel BC, Chen Z-L, Liu Y-P, Royden LH (1995) Tectonics of the Longmen Shan and adjacent regions, central China. Int Geol Rev 37:661–735

Clark MK, Royden LH (2000) Topographic ooze: building the eastern margin of Tibet by lower crustal flow. Geology 28:703–706

Clark MK, Bush JWM, Royden LH (2005) Dynamic topography produced by lower crustal flow against rheological strength heterogeneities bordering the Tibetan Plateau. Geophys J Int 162:575–590

Deng Q-D, Zhang P-Z, Ran Y-K, Yang X-P, Min W, Chu Q-Z (2002) The basic characteristics of active tectonics in China. Sci China (D) 32(12):1020–1030 **(in Chinese)**

Evariste NH, Liu G-Y, Tabod TC, Joseph K, Severin N, Alain T, Ke X-P (2014) Crustal structure beneath Cameroon from EGM2008. Geodesy Geodyn 5(1):1–10

Ji S-C, Wang Q, Sun S-S, Xu Z-Q, Li H-B (2008) Continental extrusion and seismicity in China. Acta Geol Sin 82:1144–1167 **(in Chinese with English abstract)**

Jiang W-L, Zhang J-F, Lu X-C, Lu J (2011) Crustal structure beneath Beijing and its surrounding regions from gravity data. Earthq Sci 24:299–310

Jiang W-L, Zhang J-F, Tian T, Wang X (2012) Crustal structure of Chuan-Dian region derived from gravity data and its tectonic implications. Phys Earth Planet Int 212–213:76–87

Laske G, Master G, Ma Z-T, Pasyanos M (2013) Update on CRUST1.0—a 1-degree global model of earth's crust. Geophysics Research Abstracts, vol 15, EGU2013, p 2658

Leloup PH, Lacassin R, Tapponnier P, Schärer U, Zhong D-L, Liu X-H, Zhang L-S, Ji S-C, Trinh PT (1995) The Ailao Shan-Red River shear zone (Yunnan, China), tertiary transform boundary of Indochina. Tectonophysics 251:3–84

Lou H, Wang C-Y (2005) Wavelet analysis and interpretation of gravity data in Sichuan–Yunnan region, China. Acta Seismol Sin 18(5):552–561

Mallat S (1989) A theory for multiresolution signal decomposition: the wavelet representation. IEEE Pattern Anal Machine Intell 11(7):674–693

Molnar P, England P, Martinod J (1993) Mantle dynamics, uplift of the Tibetan Plateau, and the Indian Monsoon. Rev Geophys 31:357–396

Oldenburg DW (1974) Inversion and interpretation of gravity anomalies. Geophysics 39:526–536

Oruç B (2014) Structural interpretation of southern part of western Anatolian using analytic signal of the second order gravity gradients and discrete wavelet transform analysis. J Appl Geophys 103:82–98

Parker RL (1972) The rapid calculation of potential anomalies. Geophys J R Astron Soc 31:447–455

Pavlis NK, Holmes SA, Kenyon SC, Factor JK (2012) The development and evaluation of the Earth Gravitational Model 2008 (EGM2008). J Geophys Res 117:B04406. doi:10.1029/2011JB008916

Royden LH, Burchfiel BC, King RW, Wang E, Chen Z-L, Shen F, Liu Y-P (1997) Surface deformation and lower crustal flow in eastern Tibet. Science 276:788–790

Shen Z-K, Lü J-N, Wang M, Bürgmann R (2005) Contemporary crustal deformation around the south east borderland of the Tibetan Plateau. J Geophys Res 110:B11409. doi:10.1029/2004JB003421

Shoenbohm LM, Burchfiel BC, Chen L-Z (2006) Propagation of surface uplift, lower crustal flow, and Cenozoic tectonics of the southeast margin of the Tibetan Plateau. Geology 34(10):813–816

Socquet A, Pubellier M (2005) Cenozoic deformation in western Yunnan (China–Myanmar border). J Asian Earth Sci 24:495–515

Tapponnier P, Molnar P (1977) Active faulting and tectonics of China. J Geophys Res 82:2905–2930

Tapponnier P, Peltzer G, Le Dain AY, Armijo R, Cobbold P (1982) Propagating extrusion tectonics in Asia: new insights from simple experiments with plasticine. Geology 10:611–616

Tapponnier P, Xu Z-Q, Roger F, Meyer B, Arnaud N, Wittlinger G, Yang J-S (2001) Oblique stepwise rise and growth of the Tibet Plateau. Science 294:1671–1677

Wang C-Y, Han W-B, Wu J-P, Lou H, Chan WW (2007) Crustal structure beneath the eastern margin of the Tibetan Plateau and its tectonic implications. J Geophys Res 112:B07307. doi:10.1029/2005JB003873

Wang Y-Z, Wang E-N, Shen Z-K, Wang M, Gan W-J, Qiao X-J, Meng G-J, Li T-M, Tao W, Yang Y-L, Cheng J, Li P (2008) GPS-constrained inversion of present-day slip rates along major faults of the Sichuan–Yunnan region, China. Sci China (D) 51(9):1267–1283

Wang Q-S, Teng J-W, Zhang Y-Q, Zhang X-M, Yang H (2009) The crustal structure and gravity isostasy in the middle western Sichuan area. Chin J Geophys 52(2):579–583 **(in Chinese with English abstract)**

Wang E, Meng K, Su Z, Meng Q-R, Chu J-J, Chen Z-L, Wang G, Shi X-H, Liang X-Q (2014) Block rotation: tectonic response of the Sichuan basin to the southeastward growth of the Tibetan Plateau along the Xianshuihe–Xiaojiang fault. Tectonics 33:686–717

Wu L-X, Yang M-Z, Zhao W-M, Fu R-S, Zhu L-B, Shi X-J (2011) Crust thickness inverted from multi-scale decomposition of Bouguer gravity anomalies in northeastern of Qinghai-Tibet Plateau. J Geodesy Geodyn 31(1):19–23 **(in Chinese with English abstract)**

Xu X-W, Wen X-Z, Chen G-H, Yu G-H (2008) Discovery of the Longriba fault zone in Eastern Bayan Har block, China and its tectonic implication. Sci China (D) 51(9):1209–1223

Xu Y, Hao T-Y, Li Z-W, Duan Q-L, Zhang L-L (2009) Regional gravity anomaly separation using wavelet transform and spectrum analysis. J Geophys Eng 6:279–287

Xuan S-B, Xing L-L, Tan H-B, Wang J, Shen C-Y, Li H (2012) Wavelet multi-scale decomposition of gravity field variations during period 2000 to 2007 in China mainland. J Geodesy Geodyn 32(3):7–16 **(in Chinese with English abstract)**

Yang W-C, Shi Z-Q, Hou Z-Z, Cheng Z-Y (2001) Discrete wavelet transform for multiple decomposition of gravity anomalies. Chin J Geophys 44(4):534–545 **(in Chinese with English abstract)**

Yin A, Harrison TM (2000) Geological evolution of the Himalayan-Tibetan orogen. Ann Rev Earth Planet Sci 28:211–280

Zhang P-Z, Shen Z-K, Wang M, Gan W-J, Bürgmann R, Molnar P, Wang Q, Niu Z-J, Sun J-Z, Wu J-C, Sun H-R, You X-Z (2004) Continuous deformation of the Tibetan Plateau from global positioning system data. Geology 32:809–812

Zhang G-M, Ma H-S, Wang H, Wang X-L (2005) Boundaries between active tectonic blocks and strong earthquakes in the China mainland. Chin J Geophys 48(3):602–610 **(in Chinese with English abstract)**